An efficient hybrid downscaling framework to estimate high-resolution river hydrodynamics

Zeli Tan[1], Donghui Xu[1], Sourav Taraphdar[1], Jiangqin Ma[2], Gautam Bisht[1], L. Ruby Leung[1]

[1]Pacific Northwest National Laboratory, Richland, 99352, USA

[2]College of Engineering, Georgia Institute of Technology, Atlanta, 30332, USA

Correspondence to: Zeli Tan (zeli.tan@pnnl.gov)

Abstract. Flow depth and velocity are the most important hydrodynamic variables that govern various river functions, including water resources, navigation, sediment transport, and biogeochemical cycling. Existing high-resolution flow depth simulations rely on either computationally expensive river hydrodynamic models (RHMs) or data-driven models with formidable training costs, whereas data-driven modeling of flow velocity has rarely been explored. Here, using the hybrid Low-fidelity, Spatial analysis, and Gaussian process learning (LSG) model, we developed a downscaling approach to construct high-resolution flow depth and velocity from a two-dimensional (2-D) RHM simulation at coarse resolution. The LSG models were trained and tested in an urban watershed in Houston using two different hurricane-driven flood events. The high-resolution (as fine as 30 m resolution) and low-resolution (mostly 1000 m resolution) meshes include 664,724 and 14,536 grid cells, respectively. The results showed that through downscaling, the simulation errors were reduced to less than one-fourth and one-third of the errors of the low-resolution 2-D RHM for flow depth and velocity, respectively. Our analysis further revealed that the dominant uncertainty sources of the downscaled hydrodynamics are different, with flow velocity dominated by the dimensionality reduction error, which we reduced by using a regionalized training procedure. The downscaling approach achieves an 84-fold acceleration in computational time compared to the high-resolution 2-D RHM, making high-fidelity ensemble flood modeling feasible. More importantly, the developed method provides an opportunity to couple large-scale hydrodynamical processes with local physical, chemical, and biological processes in river models.

1 Introduction

Rivers play a crucial role in water resources, navigation, sediment transport, and biogeochemical cycling (Syvitski et al., 2005; Oki & Kanae, 2006; Allen & Pavelsky, 2018; Ibáñez & Peñuelas, 2019; Mao et al., 2019; Regnier et al., 2022; Feng et al., 2023a; Rocher-Ros et al., 2023). To sustain these vital services, river flow depth and velocity must remain within normal ranges. Extreme flow depths can result in extensive fluvial flooding (Bates, 2022), whereas prolonged low flow depths jeopardize the availability of drinking and irrigation water in many regions worldwide (Gadgil, 1998; Haddeland et al., 2006). Together, flow depth and velocity are key drivers of navigation capability, sediment transport, and biogeochemical processes in rivers (Zhang et al., 2014; Raymond et al., 2016; Li et al., 2022; Sukhodolov et al., 2023). Consequently, extreme variations

30   in flow depth and velocity can lead to waterway blockage, channel aggradation or degradation, water quality deterioration, and habitat loss. River flow depth and velocity regimes are dynamic and influenced by climate change and human activities, leading many rivers to experience extreme flow conditions (Mishra & Shah, 2018). These conditions exacerbate flooding (Freer et al., 2011), degrade aquatic ecosystems (Carpenter et al., 2011; Battin et al., 2023), and diminish water supplies (Oki & Kanae, 2006). Hence, accurate prediction of river flow depth and velocity in the context of a changing climate is essential for ensuring

35   the well-being of human society (IPCC, 2021).

        Flow depth and velocity are commonly simulated using river hydrodynamic models (RHMs). Widely used RHMs are often based on one-dimensional (1-D) or two-dimensional (2-D) Saint-Venant equations, disregarding vertical variations due to the significant difference between the horizontal and vertical length scales of rivers (Li et al., 2013; Teng et al., 2017; Bates, 2022; Huang et al., 2022). Considering the low computational cost and high numerical stability, Earth system models (ESMs)

40   usually employ 1-D RHMs as the river component for large-scale and/or ensemble hydrological simulations (Li et al., 2013; Feng et al., 2024). However, they are unsuitable for high-fidelity flood simulations. This is because 1-D RHMs are solved on upscaled river networks rather than actual river reaches (Wu et al., 2011; Liao et al., 2022) and rely on uncertain parameterizations, such as the bathtub method for estimating floodplain inundation (Luo et al., 2017; Xu et al., 2022). Additionally, by oversimplifying and/or neglecting momentum transport in river channels and floodplains (Luo et al., 2017;

45   Feng et al., 2022), 1-D RHMs lack the capability to simulate fine-scale river hydrodynamics required for geomorphological and biogeochemical modeling (Hostache et al., 2014; Shabani et al., 2021). Conversely, 2-D RHMs can solve full river dynamics. When running on high-resolution meshes, they can accurately capture river flow depth and velocity (Razavi et al., 2012). Therefore, high-resolution 2-D RHMs are often referred to as high-fidelity (HF) models, whereas both 1-D RHMs and low-resolution 2-D RHMs are referred to as low-fidelity (LF) models. However, the significant computational cost of HF

50   RHMs (Teng et al., 2017; Wu et al., 2020; Ivanov et al., 2021) makes them not viable for real-time modeling and flood risk assessments through ensemble modeling, which requires hundreds or thousands of model realizations (Wu et al., 2020).

        To achieve accurate and affordable simulations of river hydrodynamics, several alternative approaches have been developed (Razavi et al., 2012). One prominent approach is the use of data-driven models to emulate the behaviors of HF RHMs (Ivanov et al., 2021; Tran et al., 2023). With the rapid advancement of machine learning (ML) techniques, ML-based

55   emulators have been increasingly employed in hydrological sciences, including applications such as modeling runoff (Gao et al., 2020), evapotranspiration (Hu et al., 2021), inundation (Xie et al., 2021), lake-river interactions (Liang et al., 2018; Huang et al., 2022), reservoir operations (Zhang et al., 2018; Yang et al., 2019), streamflow (Ha et al., 2021; Sikorska-Senoner & Quilty, 2021), groundwater (He et al., 2020; Wunsch et al., 2022), and water quality (Chen et al., 2020; Saha et al., 2023). These studies have demonstrated that, once trained under extensive conditions, the computationally efficient ML models can

60   mimic numerical models. However, general ML-based emulators often lack the enforcement of physical laws, such as the conservation of mass and momentum (Konapala et al., 2020; Karniadakis et al., 2021), resulting in poor transferability to out-of-sample conditions in nonstationary systems (Young et al., 2017; Konapala et al., 2020), such as streamflow in a changing climate. To address this limitation, variants like physics-informed neural networks have been developed, embedding physical

laws (e.g., Saint-Venant equations) into their cost functions to constrain ML solutions. However, the incorporation of physical laws tends to reduce the training efficiency of ML models (Feng et al., 2023b).

The second approach is to downscale the low-resolution RHM simulation onto a finely discretized grid (Wilby & Dawson, 2013; Feng et al., 2023b). For instance, Bermúdez et al. (2020) created high-resolution inundation maps by simply interpolating flow depth computed from a LF RHM onto a high-resolution digital elevation model (DEM). Recently, more advanced downscaling methods have been developed using various ML techniques to reproduce the detailed spatial and temporal features of high-resolution river hydrodynamics (Carreau & Guinot, 2021). Notably, Fraehr et al. (2022) developed a novel downscaling method based on the hybrid Low-fidelity, Spatial analysis, and Gaussian process learning (LSG) model. This method demonstrated promising accuracy in simulating the dynamic behavior of flood inundation, such as the rising and recession components and hysteresis, at the computational cost of a low-resolution 2-D RHM (Fhraehr et al., 2022). Later, Fraehr et al. (2023a) extended the approach for fast and accurate simulations of not only high-resolution flood extent but also high-resolution flow depth. Additionally, the LSG-based downscaling model can support both structured and unstructured grids, a significant advantage as modern 2-D RHMs increasingly adopt unstructured grids for fine-scale modeling (Begnudelli & Sanders, 2006; Kim et al., 2012). However, like Fraehr et al. (2022 & 2023a), existing research on hydrodynamic model downscaling is mostly flood prediction oriented and thus has focused entirely on flood extent and magnitude, while ignoring flow velocity. This overlook is problematic from two perspectives. First, it could increase the uncertainty of flood risk simulations because flood velocity is a critical factor for human safety risks in flood events (Russo et al., 2013). Moreover, as discussed earlier, in the context of Earth system modeling, without accurate simulations of flow velocity, it is not possible to realistically predict how river functions respond to environmental stresses. While Fraehr et al. (2022 & 2023a) only applied the LSG-based downscaling approach for inundation extent and depth, this method should theoretically also be applicable for flow velocity. This is because the mass and momentum of river flow are governed by the unified shallow water equations and driven by the same environmental factors. However, such an application has not yet been explored.

In this study, we develop an LSG-based downscaling approach to achieve accurate simulations of high-resolution river flow depth and velocity at the computational cost of a low-resolution 2-D RHM. Compared to Fraehr et al. (2022 & 2023a), the main innovation of our study is to test and enhance the LSG-based downscaling approach for high-resolution flow velocity downscaling. This extension of the LSG-based downscaling approach is expected to greatly broaden its usefulness for Earth system modeling. Besides, we test the effectiveness of the downscaling method in an urbanized watershed in the Houston area using data from two different extreme hurricane events. Together with Fraehr et al. (2022 & 2023a), our independent validation in a different environment would help examine whether the LSG-based downscaling approach has broad geographical applicability. Furthermore, based on this downscaling method, we propose a new paradigm to couple large-scale hydrodynamical processes with local detailed physical, chemical, and biological processes in river models. The remainder of this paper is organized as follows: Section 2 describes the downscaling method and the configurations of the high-resolution and low-resolution 2-D RHMs for the study events; Section 3 highlights the main results; Section 4 discusses the implications of the results, outlines the limitations of our approach, and introduces the new paradigm; and Section 5 concludes the paper.

2 Materials and Methods

2.1 LSG model

100   For the LSG model, the underlying principle is that the dynamics of flow depth and velocity can be approximated by a limited number of temporal and spatial modes due to their strong spatial pattern controlled by topography. The LSG model consists of a LF RHM, key spatial modes extracted from a HF RHM, and a sparse Gaussian Process (GP) emulator model. It uses the LF RHM as a transfer function to capture the dynamics and spatial correlation of river flow. The key temporal features of the LF RHM outputs are extracted through an Empirical Orthogonal Function (EOF) analysis based on the extracted spatial

105   features from the HF RHM, thereby allowing the use of a Sparse GP model to convert the LF data to HF data via conversion of the extracted temporal features. The LSG model can reconstruct high-fidelity river hydrodynamics for two reasons. First, the accurate spatial correlations of river hydrodynamics are preserved due to the use of the key spatial modes from the HF model, which are assumed to not vary by events. Second, the Sparse GP model is efficient and effective in reconstructing the dynamics of HF data. In this study, we used the same 2-D shallow water equations to construct the LF and HF RHMs (described

110   later). The only difference between them is the spatial resolution, with the coarse mesh adopted by the LF model reducing the simulation accuracy. We followed the procedure described by Fraehr et al. (2022, 2023a) to train and apply LSG models for river flow depth and velocity downscaling (Fig. 1), with any deviations from the general procedure specifically highlighted.
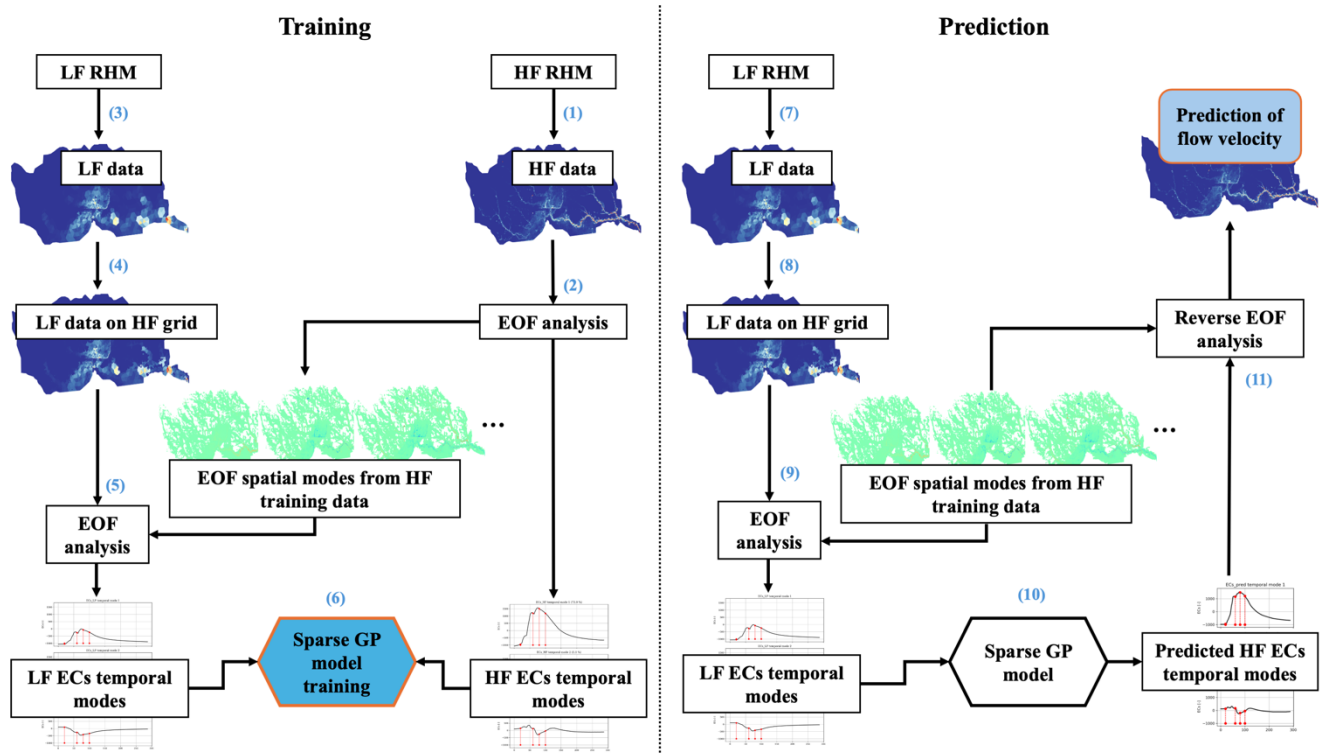
Figure 1: Workflow of training the LSG model and using the trained model to predict high-resolution river hydrodynamics.

For training, we first run the HF RHM over the study domain for a training flood event (Step 1) and derive the spatial EOF modes and the temporal expansion coefficients (ECs) modes of this HF simulation through the EOF analysis (Step 2) as defined in Eq. (1).

$$D_{HF} = U_{HF} \cdot C_{HF} \approx \sum_{k=1}^{K} U_{HF}(k,:) \cdot C_{HF}(:,k), \tag{1}$$

where D_{HF} is a $T \times N$ matrix containing simulated HF flow depth or velocity (T is the number of timesteps in the training data and N is the number of wet cells) that have been detrended (Fraehr et al., 2023a), U_{HF} is a $T \times N$ matrix each row of which is an EOF spatial map, C_{HF} is a $T \times T$ matrix each column of which corresponds to an EC temporal function, and K is the number of significant modes determined by both North's test (North et al., 1982) and Kaiser's Rule (Kaiser, 1960).

For the training phase, we also run the LF RHM for the training event (Step 3) and interpolate the simulated flow depth and velocity from the coarse mesh used by the LF model to the fine mesh used by the HF model (Step 4). Notably, we improved the nearest neighbor interpolation method adopted by Fraehr et al. (2023a) by accounting for mass conservation. While our improved method still assumes a homogeneous water level within a coarse grid cell, it ensures that the sum of interpolated water volume in fine grid cells equals the water volume in the coarse grid cell. Additionally, we ensure that the interpolation of flow velocity only occurs at wet grid cells where the water depth is greater than 3 cm (Fhraehr et al., 2023a). Another difference is that we do not apply area-based weights to D_{HF} before the EOF analysis, as Fraehr et al. (2023a) recommended. This is because we are more interested in the flow depth and velocity of river channels and nearby floodplains that are represented by smaller grid cells in our fine mesh (Fig. 2).

Next, we perform the EOF analysis on the interpolated LF flow depth and velocity to derive the temporal EC modes of the LF simulation (Step 5). Using the extracted high-resolution EOF spatial modes from Step 2, the extracted temporal ECs are defined in Eq. (2).

$$C_{LF} = D_{LF} \cdot U'_{HF}, \tag{2}$$

where C_{LF} is a $T \times T$ matrix containing the LF ECs, D_{LF} is a $T \times N$ matrix corresponding to the interpolated LF flow depth or velocity simulations, and U'_{HF} is the transpose of U_{HF}. In the final step of training, we use the derived LF and HF temporal ECs to train a Sparse GP model (Rasmussen & Williams, 2006) that can predict the HF ECs from the LF ECs (Step 6). For flow depth and velocity, the training of the Sparse GP models is performed independently.

For prediction, only the low-cost LF RHM simulations are needed (Fig. 1). While Steps 7 to 9 essentially replicate Steps 3 to 5, the difference is that Steps 7 to 9 are applied to a new LF simulation that is run for an unseen flood event. After the new LF ECs are retrieved following the EOF analysis in Eq. (1) using the spatial EOF modes derived in Step 2, they are fed into the trained Sparse GP model to predict the new HF ECs (Step 10). Finally, the predicted HF ECs are combined with the EOF spatial modes from Step 2 to reconstruct the HF flow depth and velocity simulations based on the reverse EOF analysis (Step 11) as defined in Eq. (3).

$$\widehat{D_{LSG}} = \sum_{k=1}^{K} U_{HF}(k,:) \cdot \widehat{C_{LSG}}(:,k), \tag{3}$$

where $\widehat{D_{LSG}}$ is the predicted high-resolution flow depth or velocity, and $\widehat{C_{LSG}}$ is the predicted HF temporal ECs. More details of the workflow can be found in Fraehr et al. (2022 & 2023a).

The downscaling error consists of two major components: the error from dimensionality reduction and the error from the LSG model. According to Eq. (1), the error from dimensionality reduction ER_{DR} can be defined as: $ER_{DR} = D_{HF} - \sum_{k=1}^{K} U_{HF}(k,:) \cdot C_{HF}(:,k)$. According to Eq. (3), the error from the LSG model ER_{LSG} can be defined as: $ER_{LSG} = \sum_{k=1}^{K} U_{HF}(k,:) \cdot C_{HF}(:,k) - \sum_{k=1}^{K} U_{HF}(k,:) \cdot \widehat{C_{LSG}}(:,k)$.

2.2 Study site and flood events

We used the Hurricane Harvey flood event (hereafter referred to as Harvey) in the Houston area as a case study. On August 26, 2017, Harvey made landfall along the mid-Texas coast as a Category 4 hurricane. As one of the worst hurricanes to hit the United States in recent history, Harvey brought record-breaking rainfall across the Houston metropolitan area (Van Oldenborgh et al., 2017), causing more than 80 fatalities and over $150 billion in economic losses, mostly due to extraordinary flooding (Emanuel, 2017; Balaguru et al., 2018). Specifically, we selected the Buffalo Bayou at Turning Basin as the study domain (Fig. 2), where the selected RHM was recently validated at different resolutions (Xu et al., 2025).
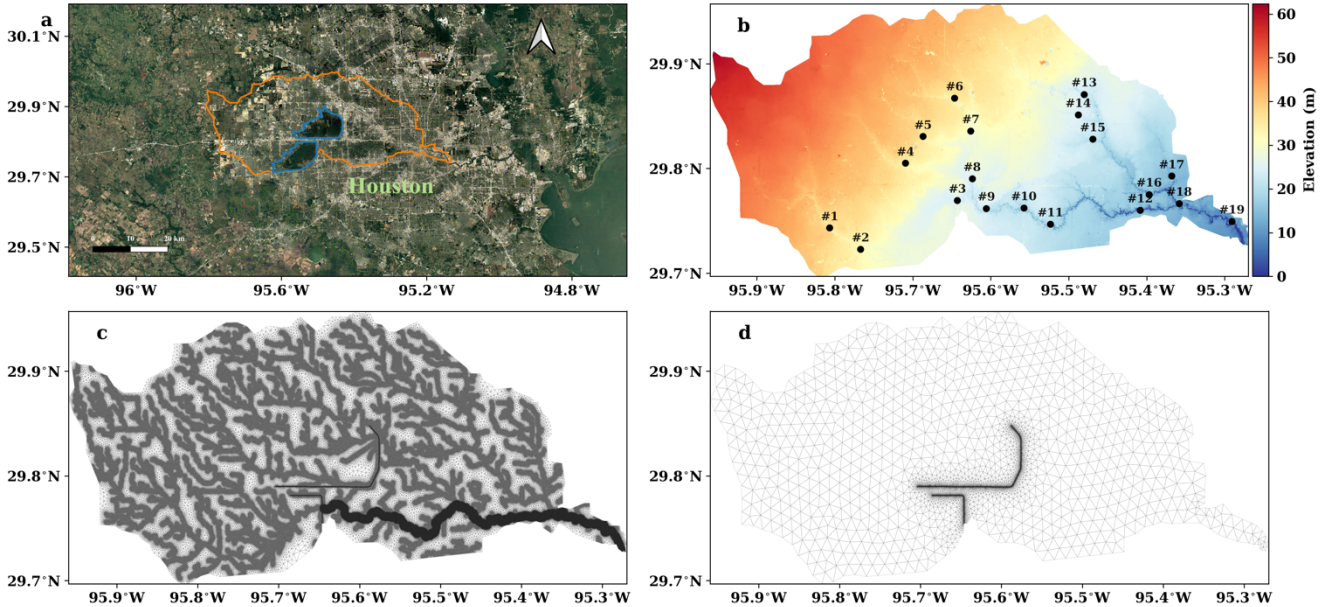
Figure 2: Study domain (a), topography (b), high-resolution mesh (c), and coarse-resolution mesh (d) for river hydrodynamics simulations in the Turning River basin. The river basin boundary and the boundaries of two reservoirs in the basin are highlighted in orange color and blue color, respectively, in (a) and the black dots in (b) show the locations of the USGS gauges (Table S1) along with their gauge number. The basemap in (a) is extracted from Google Imagery @2024 TerraMetrics, Map data @2024. The seemingly thick bold lines in (c) are dense grid cells for river channels. The seemingly black lines in (d) are dense grid cells for the dams of the two reservoirs, which can also be seen in (c).

Precipitation during Hurricane Harvey (Fig. 3) is extracted from the 1-km resolution Multi-Radar Multi-Sensor (MRMS) precipitation dataset, which has a native temporal resolution of two minutes (Zhang et al., 2016). To demonstrate the effectiveness of our downscaling approach for ensemble flood projections, we use a projected hurricane event (Hurricane

Harvey-like) under the high warming scenario — Shared Socioeconomic Pathway SSP5-8.5 — as a test case (Fig. 3). The future hurricane is simulated using the Energy Exascale Earth System Model (E3SM) with the novel Simple Cloud-Resolving E3SM Atmosphere Model (SCREAM) configuration (Caldwell et al., 2021; Donahue et al., 2024). SCREAM is a global atmospheric circulation model with a non-hydrostatic dynamical core and parameterizations for atmospheric radiative transfer, cloud microphysics, and boundary layer clouds and turbulence (Caldwell et al., 2021). The SCREAM domain features a regionally refined mesh (RRM) with 3.25 km grid spacing over the east coast of the United States, including the Gulf of Mexico and a significant part of the Atlantic Ocean, within a global domain that has 25 km grid spacing outside the RRM. Nudging is applied to grid cells outside the RRM to constrain the atmospheric circulation using the European Centre for Medium-Range Weather Forecasts (ECMWF) Reanalysis version 5 (ERA5) data (Hersbach et al., 2020). These features enable SCREAM to capture fine-scale extreme weather events, accurately resolve coastal areas and mountainous regions, and properly represent convective clouds, which are major sources of climate model uncertainty (Sherwood et al., 2014). SCREAM is coupled with the E3SM Land Model (ELM), while sea surface temperature and sea ice extent are prescribed based on ERA5.

In the historical simulation, SCREAM is initialized using ERA5 to simulate Hurricane Harvey (hereafter referred to as the SCREAM simulation). To simulate how Hurricane Harvey will behave under future conditions, a storyline simulation using SCREAM is performed (hereafter referred to as the Pseudo Global Warming, PGW, simulation). In the PGW simulation, the initial conditions and nudging data from ERA5 are perturbed by adding the mean monthly changes derived from a multi-model ensemble of climate simulations from the Coupled Model Intercomparison Project Phase 6 (CMIP6) to represent the mean climate change under the SSP5-8.5 scenario by the end of the 21st century (2079-2099) compared to the historical climate at the end of the 20th century (1990-2010). A similar perturbation is also applied to ELM for the PGW simulations.

SCREAM can successfully predict the heavy precipitation during Harvey's landfalls in Texas on August 26, but its simulated precipitation during the subsequent landfalls on August 27 and 28 is relatively muted (Fig. 3a), a well-known challenge even for many weather forecasting models (Wang et al., 2018; Yang et al., 2019). Considering the high computational cost of the SCREAM runs, we conducted three PGW simulations to drive the ensemble flood projections. These simulations, each with slightly different initial conditions, represent the uncertainty of the hurricane projection due to internal variability at the weather timescale (Fig. 3f). One PGW simulation is selected for LSG model validation. Its temporal and spatial patterns of precipitation are shown in Figs. 3a, 3b, and 3d, which are significantly different from the patterns of the benchmark precipitation (Figs. 3a, 3b, and 3c) selected for LSG model training. The simulation differences reflect model uncertainty and the effects of climate change on the hurricane. Correspondingly, the simulated peak water depth from the HF RHM using the benchmark precipitation is significantly larger than that using the PGW precipitation (Fig. 3e). The significant difference in the benchmark and PGW precipitation as well as that in flood simulations supports the use of the latter as an out-of-sample test case, relevant for projecting future flooding. Additionally, the choice of a PGW flood event over a historical flood event for validation aligns better with the application scenarios of our downscaling method that are ensemble flood projections.
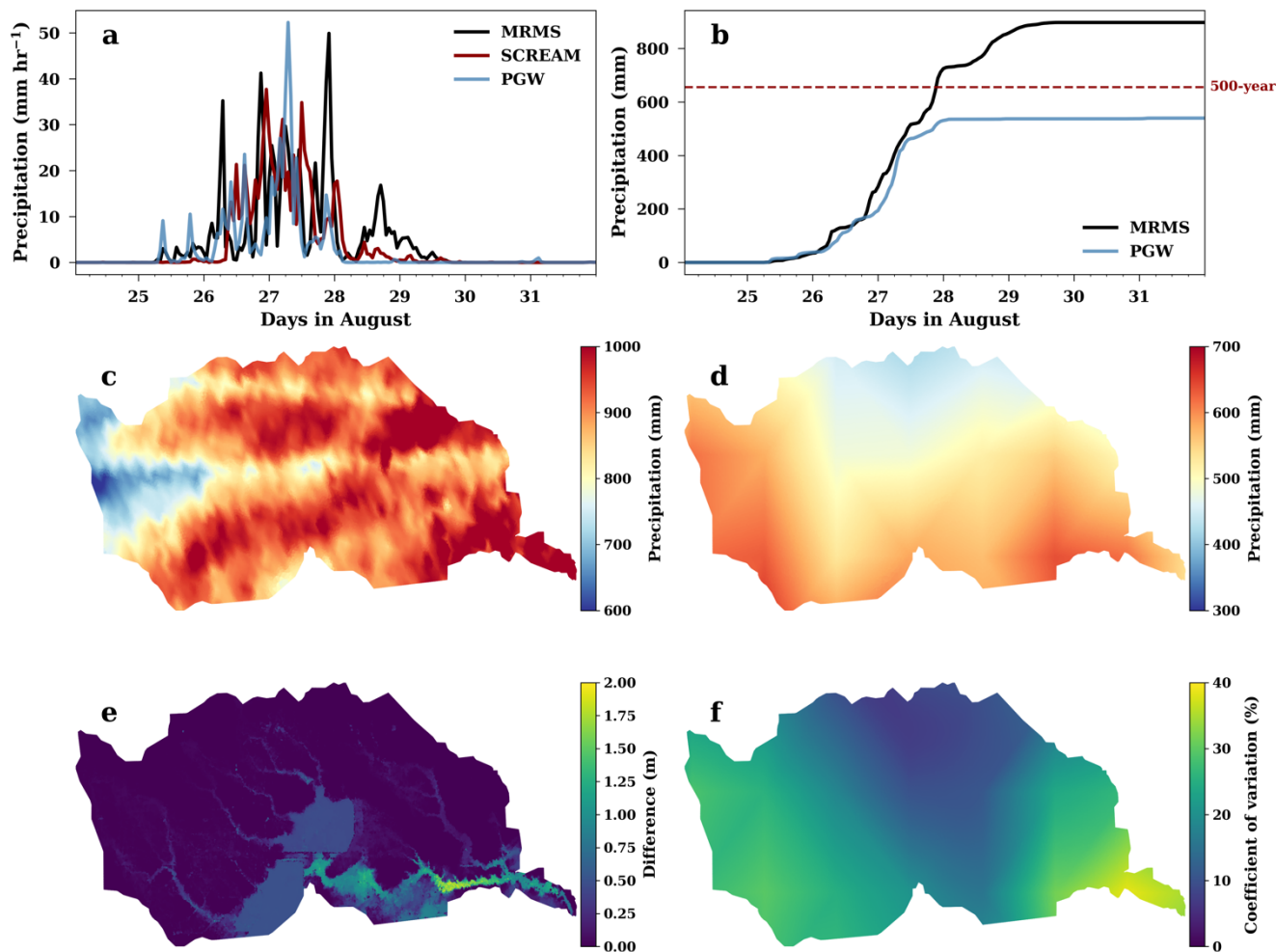
Figure 3. Comparison of the observed (MRMS) and simulated hourly precipitation during Harvey under the observed historical (SCREAM) and projected future (PGW) conditions (a), comparison of the cumulative MRMS and PGW precipitation (b), and maps of the observed cumulative precipitation during Harvey (c), the cumulative precipitation of the PGW simulation selected for the LSG model validation (d), the difference between the simulated peak water depth from the HF RHM using MRMS and that using the PGW precipitation (e), and the coefficient of variation (CV) of the PGW simulated cumulative precipitation ensemble (f) in the study domain. The 7-day total precipitation for the 500-year return period in the Houston area is marked in (b).

2.3 River Hydrodynamic Model

In this study, we chose the 2-D Overland Flow Model (OFM; Kim et al., 2012) for river hydrodynamics modeling, which was recently validated for the Harvey flood simulations (Xu et al., 2025). In brief, OFM is a finite volume model that implements the first-order Godunov-type upwind scheme on a triangular mesh and uses Roe's approximate Riemann solver to compute fluxes between grid cells (Begnudelli & Sanders, 2006). Later, Ivanov et al. (2021) improved OFM's computational efficiency by using the Portable, Extensible Toolkit for Scientific Computation (PETSc; Balay et al., 2019) software for model

parallelization. Mathematically, OFM solves the 2-D shallow water equations, which include the terms of advection, bottom friction, and gravity but ignore the terms of Coriolis and viscous forces (Begnudelli & Sanders, 2006):

$$\frac{\partial h}{\partial t} + \frac{\partial (uh)}{\partial x} + \frac{\partial (vh)}{\partial y} = q, \tag{4}$$

$$\frac{\partial (uh)}{\partial t} + \frac{\partial \left(u^2 h + \frac{1}{2} g h^2\right)}{\partial x} + \frac{\partial (uvh)}{\partial y} = -gh \frac{\partial z_b}{\partial x} - C_D u \sqrt{u^2 + v^2}, \tag{5}$$

$$\frac{\partial (vh)}{\partial t} + \frac{\partial (uvh)}{\partial x} + \frac{\partial \left(v^2 h + \frac{1}{2} g h^2\right)}{\partial y} = -gh \frac{\partial z_b}{\partial y} - C_D v \sqrt{u^2 + v^2}, \tag{6}$$

where t is the time (s), h is the flow depth (m), u and v are the water velocity (m s^{-1}) in the x and y direction under the Cartesian coordinate system, q is the excess precipitation rate (m s^{-1}), g is the gravitational acceleration constant (m s^{-2}), z_b is the bed elevation (m), and C_D is the bed drag coefficient derived from Manning's roughness n as $C_D = gn^2 h^{-1/3}$.

We configure the OFM model on two variable-resolution meshes, with the high-resolution configuration serving as the HF RHM and the low-resolution configuration as the LF RHM. The variable-resolution meshes are generated using a Delaunay-based unstructured mesh generator, JIGSAW (Engwirda, 2017), which can refine topographic features important for shaping river flow regimes, such as river channels (Kim et al., 2022; Xu et al., 2022), floodplains (Yamazaki et al., 2011; Schrapffer et al., 2020), and water management structures (Schmutz & Moog, 2018). Specifically, the high-resolution mesh has 664,724 grid cells over the study domain, representing the main channels, tributaries, dams, and other regular cells with resolutions of 30 m, 60 m, 30 m, and 1000 m, respectively. In contrast, the low-resolution mesh has only 14,536 grid cells over the study domain, representing the main channels, tributaries, and other regular cells with a uniform resolution of 1000 m (except for dams, which are resolved at 30 m) (Fig. 2). In both the high-resolution and low-resolution meshes, the areas around two flood control reservoirs, Addicks and Barker's Reservoir (Fig. 2), are refined to ensure more accurate flood simulations. As indicated in Xu et al. (2025), even though the simulation of streamflow at the outlet is only moderately degraded, the use of a coarser mesh severely deteriorates the model performance in simulating inundation. The 30-meter resolution Digital Elevation Model (DEM) from the National Elevation Database (NED) was used to construct the topography of the RHM meshes.

To force the OFM, the MRMS precipitation data are upscaled from their native temporal resolution to an hourly time step and spatially interpolated to the variable-resolution mesh cells using the nearest neighbor interpolation method. Similarly, the hourly SCREAM simulation data are spatially interpolated to the variable-resolution mesh cells using the nearest neighbor method before being used to force the OFM.

2.4 Validation of downscaled hydrodynamics

Validation of the downscaling method uses the "perfect prognosis" approach in which the HF RHM simulation is the target for the downscaled flow depth and velocity that uses the LF RHM simulated flow depth and velocity as the input. This validation strategy allows one to focus on evaluating the downscaling method without the influence of the RHM or observation errors and has been widely adopted in climate downscaling (Denis et al. 2002) as well as hydrological and hydrodynamic

downscaling (Carreau & Guinot, 2021; Feng et al., 2023b) when both low- and high-resolution simulations are available. Therefore, in this study, good agreement between the downscaled flow depth and velocity with the high-resolution simulations from the HF RHM is a demonstration of the effectiveness of the downscaling method.

In the study, the accuracy of the downscaled hydrodynamics is evaluated using multiple metrics. Using the HF simulation as the reference, we calculate the root-mean-square-error (RMSE) of the simulated hourly flow depth and velocity at each grid cell during the flood event and the absolute bias of the simulated flow depth and velocity at each grid cell during the flood peak. These two metrics are used to evaluate the spatial uncertainty of the downscaled estimates. The average RMSE of all the grid cells is also calculated to highlight the overall uncertainty of the downscaling. The temporal uncertainty of the downscaled hydrodynamics is assessed using the Kling-Gupta efficiency (KGE) (Gupta et al., 2009) which can evaluate the bias, correlation, and error variability of the downscaling comprehensively. The KGE is calculated at 19 USGS gauges (Figure 2) which have been previously used to validate the HF RHM (Xu et al., 2025).

3 Results

3.1 Validation of downscaled flow depth

The trained LSG models can accurately predict the spatial and temporal variabilities of flow depth (Figs. 4–5) and velocity (Figs. 6–7) for the PGW flood event. First, the results confirm the effectiveness of the EOF analysis in extracting the significant spatial and temporal modes of the 2-D shallow water equations (Figs. S4–S5). Notably, as indicated by the proportion of variance explained by the specific modes, the significant modes of flow velocity (Fig. S5) are less representative of its variability compared to those of flow depth (Fig. S4), likely due to the higher nonlinearity of flow velocity simulations. Second, the trained LSG models perform remarkably well in reconstructing the HF ECs of river hydrodynamics from the LF ECs for both the training (Figs. S6–S7) and prediction phases (Figs. S8–S9). This performance is achieved despite substantial distinctions between the HF and LF ECs. Consequently, the spatial and temporal features of the high-resolution flow depth and velocity are well reproduced for both the training (Figs. S10–S13) and prediction phases (Figs. 4–7), even though they are forced by two distinct hurricane events (Fig. 3).

During the PGW flood, using the HF simulation as the reference, the average RMSE of the downscaled flow depth is 0.07±0.1 m (Fig. 4b), which is less than one-fourth of the average RMSE (0.3±0.6 m) of the simulated LF flow depth (Fig. 4a). The downscaling achieves impressive error reductions in river channels (particularly downstream reaches), the nearby floodplains, and the two reservoirs (Fig. 4), which are flood-prone areas that have been deliberately refined in the high-resolution mesh (Fig. 2c). By downscaling, the detailed longitudinal variations of flow depth in the HF simulation (Fig. 4g) are precisely reproduced (Fig. 4d) during the peak flood period (near 01:00 am, August 27). Even very small ponding grid cells, which are barely seen in the LF simulation (Fig. 4c), are recovered (Fig. 4d). Compared to the LF simulation, the downscaled flow depth is highly consistent with the HF simulation at the peak flood time, with the bias range (from the 10th percentile to the 90th percentile) reduced from [-0.2 m, 0.3 m] (Fig. 4e) to [-0.04 m, 0.06 m] (Fig. 4f). Generally, the

downscaling reduces the underestimation and overestimation of the LF simulated flow depth in river channels and floodplains, respectively, likely due to the use of the HF EOFs (Fig. S4).
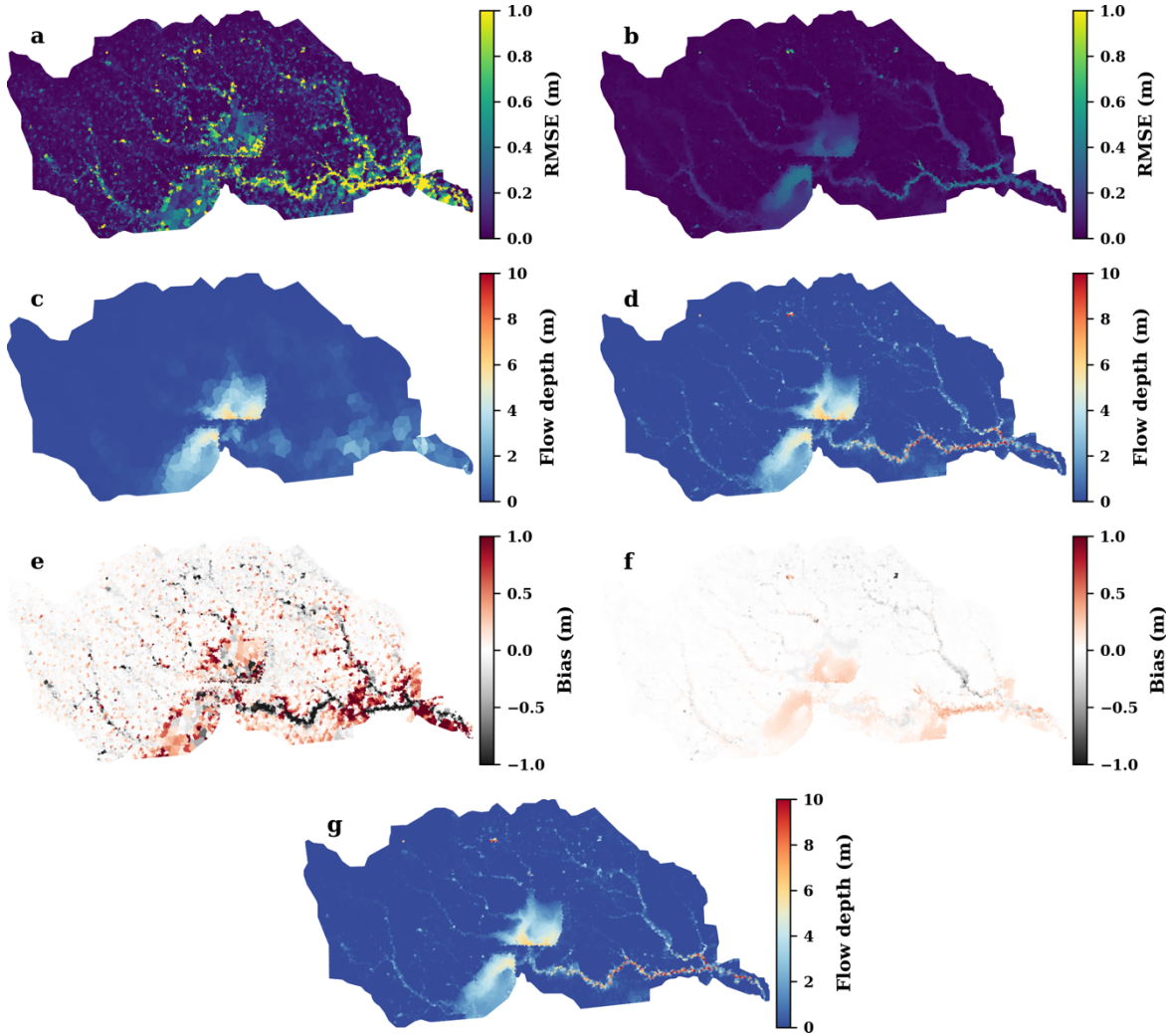
Figure 4. Root-mean-square-error (RMSE) of the LF simulated (a) and downscaled flow depth (b) for the entire PGW event, the LF simulated (c) and downscaled flow depth (d) at 01:00 am, August 27 (the peak flood time), the bias of the LF simulated (e) and downscaled flow depth (f) at the peak flood time, and the HF simulated flow depth (g) at the peak flood time. RMSE and bias are calculated by treating the HF simulation as "ground truth".

The downscaling approach also performs promisingly in reproducing the temporal variability of the HF simulated flow depth at the selected USGS gauges (Fig. 5). The downscaled flow depth achieves KGE ≥ 0.5 (good performance) at all gauges except Gauge #14, where small inundation occurs. In contrast, the LF simulation only achieves KGE ≥ 0.5 at two gauges but exhibits poor performance (KGE < -0.41; Knoben et al., 2019) at three gauges, whereas the performance at the other gauges is barely acceptable (-0.41 < KGE < 0.5). Notably, for four gauges (#3, #7, #8, and #19), the downscaling approach achieves

KGE ≥ 0.9 (excellent performance). Not only does the downscaling reduce the severe biases of the LF simulation at nearly all gauges, but it also recovers dynamics not captured by the LF simulation, such as the second peak flow depth at Gauge #18.
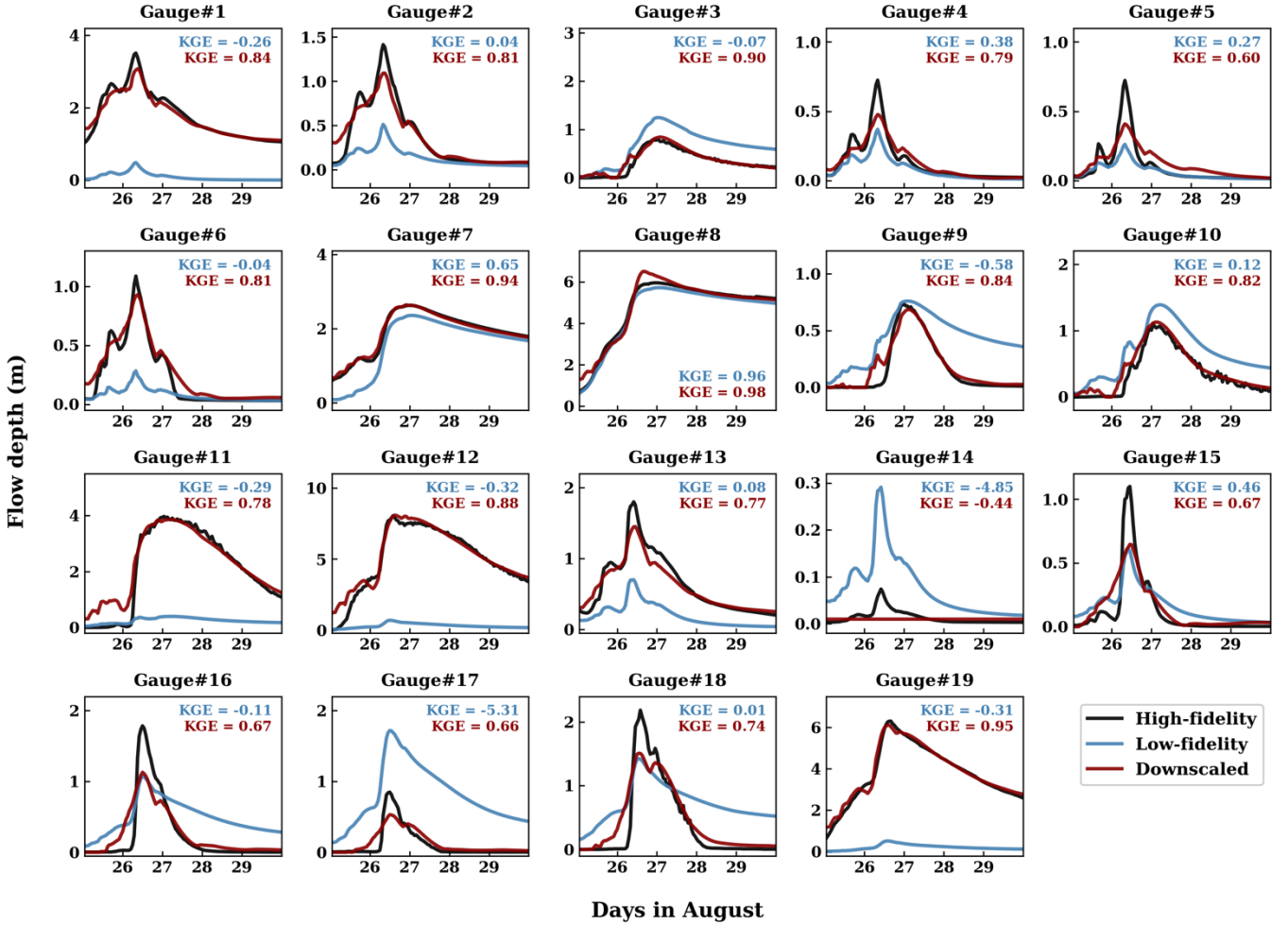
Figure 5. Comparison of the HF simulated, LF simulated, and downscaled flow depth at the selected USGS gauges during the PGW event.

3.2 Validation and enhancement of downscaled flow velocity

Likewise, the downscaled simulations provide accurate representations of the spatial and temporal variabilities of flow velocity during the PGW flood (Figs. 6–7). The downscaling significantly reduces the average RMSE of simulated flow velocity from 0.7±1.9 m s^{-1} (Fig. 6a) to 0.2±0.6 m s^{-1} (Fig. 6b). Compared to flow depth, the error reduction in flow velocity is more concentrated in the river channels, possibly reflecting the larger gradients of flow velocity from river channels to the nearby floodplains. Like flow depth, the downscaling successfully recovers the detailed longitudinal variations of flow velocity in the HF simulation (Fig. 6g), as well as the river flow in small inundated areas during the peak flood period (Fig. 6d). The

method also yields substantial reductions in the estimation bias at the peak flood time, from [-0.4 m s⁻¹, 0.3 m s⁻¹] (Fig. 6e) to [-0.07 m s⁻¹, 0.05 m s⁻¹] (Fig. 6f).

305
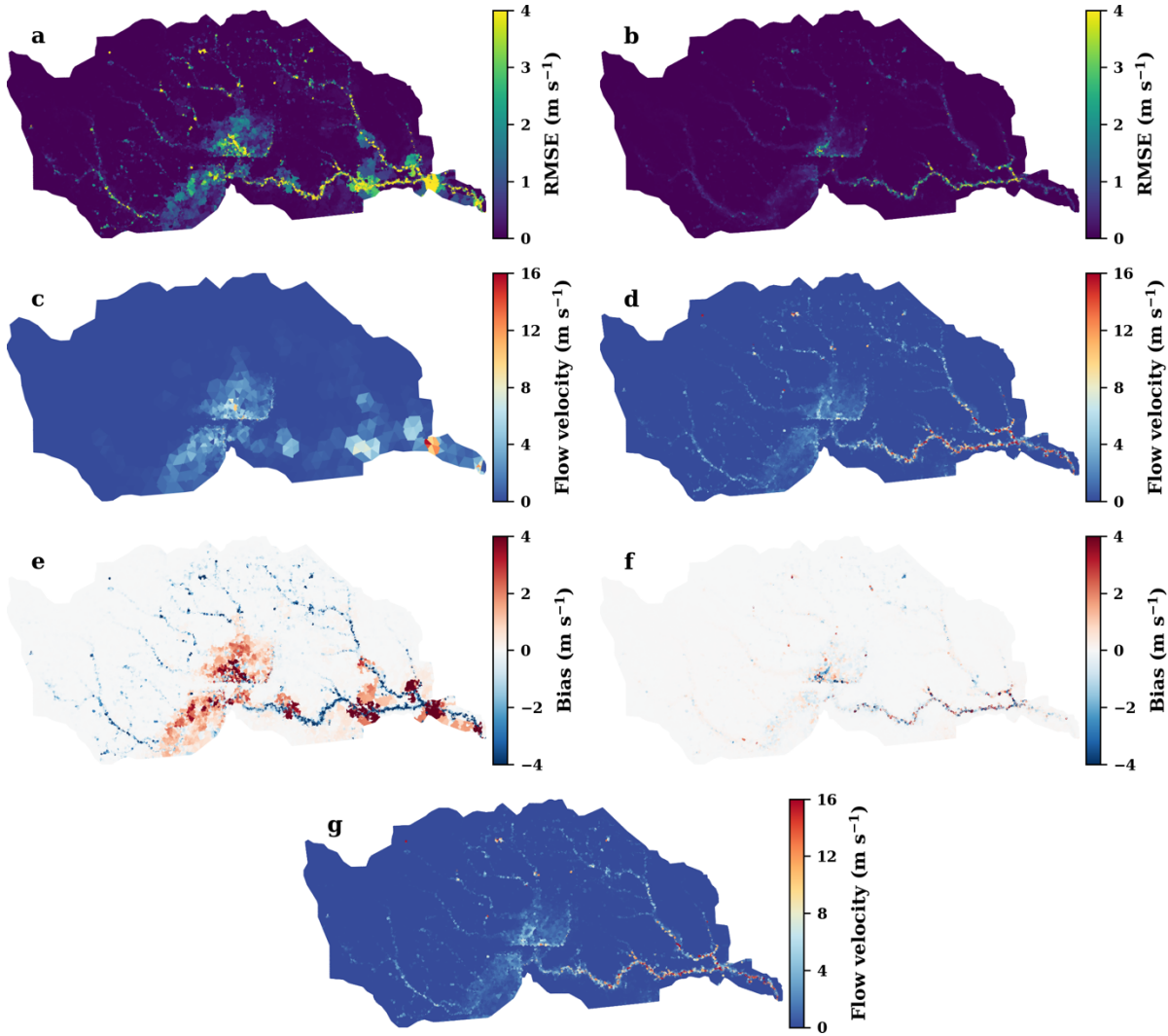
Figure 6. RMSE of the LF simulated (a) and downscaled flow velocity (b) for the entire PGW event, the LF simulated (c) and downscaled flow velocity (d) at 01:00 am, August 27 (the peak flood time), the bias of the LF simulated (e) and downscaled flow velocity (f) at the peak flood time, and the HF simulated flow velocity (g) at the peak flood time. RMSE and bias are calculated by treating the HF simulation as "ground truth".

310   The downscaling also produces more consistent temporal variability of flow velocity compared with the HF simulation at the selected USGS gauges (Fig. 7). The downscaled flow velocity achieves KGE ≥ 0.5 (good performance) at 15 gauges and KGE ≥ 0.9 (excellent performance) at two gauges (#11 and #16). In contrast, the LF simulation only achieves KGE ≥ 0.5 at Gauge #8 but exhibits unacceptable performance (KGE < -0.41) at nine gauges. However, despite its superiority to the LF simulation, the downscaled flow velocity does not perform as well as the downscaled flow depth at many of the study gauges.

315 For instance, it fails to capture the velocity spike at Gauge #1 and greatly underestimates the velocity peaks at several other gauges (e.g., #2, #4, and #8). The downscaled solutions also struggle to reproduce the high-frequency fluctuations of flow velocity, such as at Gauges #12 and #18. Analysis of the error sources indicates that for the downscaled flow velocity, the error from dimensionality reduction ER_{DR} is substantially larger than the LSG model error ER_{LSG}, while for the downscaled flow depth, ER_{LSG} is dominant (Fig. 8). First, this result aligns with the EOF analysis (Fig. S5), which shows the higher nonlinearity

320 of flow velocity simulations. Second, this implies that reducing ER_{DR} is crucial for more accurate flow velocity downscaling.
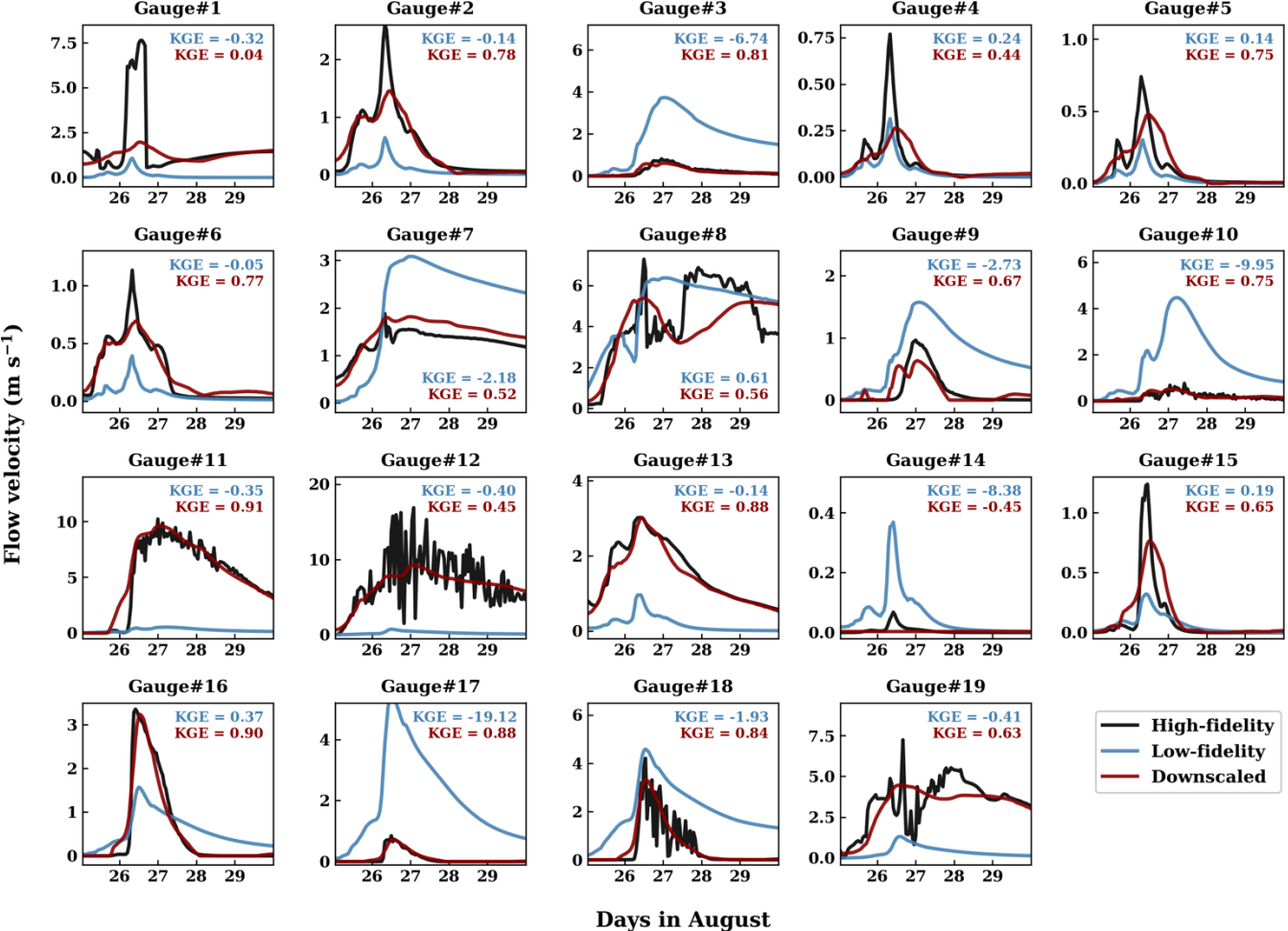
Figure 7. Comparison of the HF simulated, LF simulated, and downscaled flow velocity at the selected USGS gauges during the PGW event.
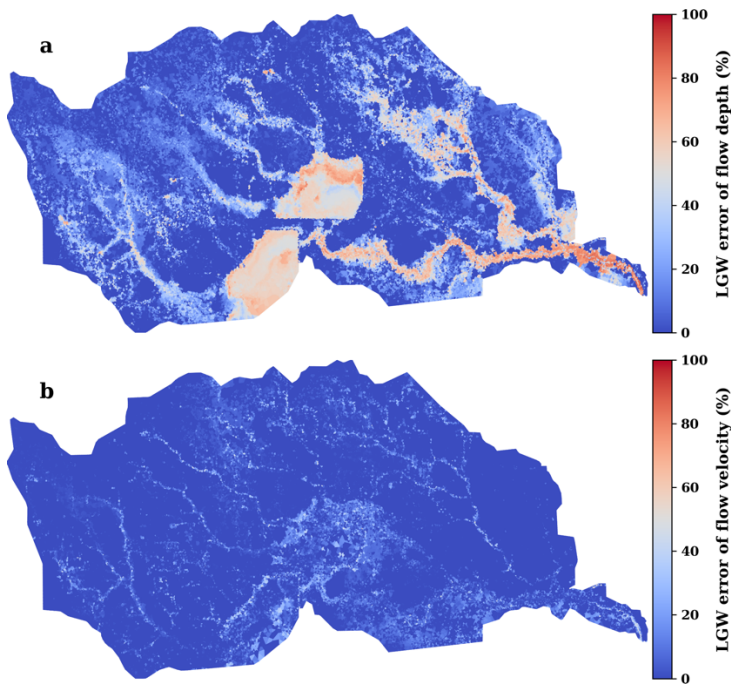
Figure 8. Percentage of flow depth (a) and velocity (b) downscaling uncertainty that can be explained by the error from the LSG model.

A possible way to reduce ER_{DR} is to regionalize the training of the LSG model in a smaller domain that focuses on a specific geographic feature. This approach can prevent locally important EC modes from being filtered out in large-scale EOF analyses (see Fraehr et al. (2023a) for North's test and Kaiser's Rule). Notably, this treatment does not require new model simulations and follows the same procedure outlined in Fig. 1. We selected Gauge #1, where the whole-domain downscaling fails to reproduce the peak flow velocity simulated by the HF model. By training a new LSG model over a smaller area encompassing the gauge (Fig. S14), the downscaled simulation aligns with the HF model for predicting the flow velocity spike on August 26 (Fig. 9). For the PGW event, the KGE for the simulated flow velocity increases significantly from 0.04 to 0.61. The regionalized training also slightly improves the accuracy of the downscaled flow depth at Gauge #1, with KGE increasing from 0.81 to 0.96. The smaller effect of regionalized training on flow depth is expected because our error analysis indicates that the uncertainty of the downscaled flow depth is only minorly contributed by ER_{DR} (Fig. 8).
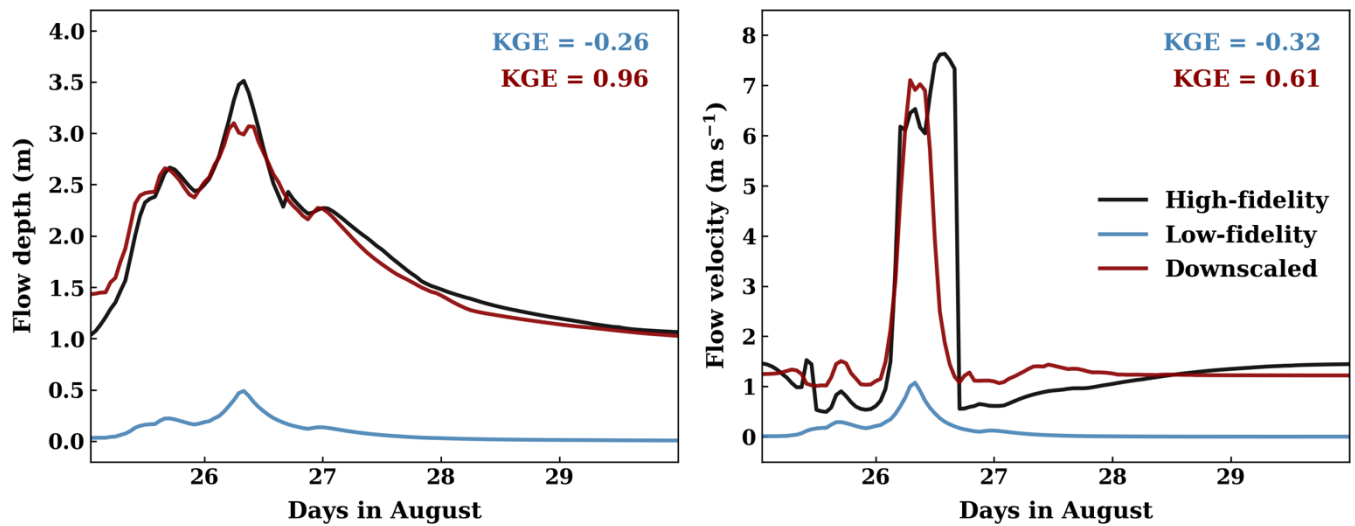
Figure 9. Comparison of the HF simulated, LF simulated, and downscaled flow depth and velocity at Gauge #1 during the PGW event with training LSG models in a focused area around the gauge (Fig. S14).

3.3 Ensemble inundation downscaling

Because the training of the LSG model can be completed within minutes, the computational cost of our downscaling approach depends solely on the computational time needed for the RHM simulations. For the 13-day PGW simulations, when running on Intel Xeon Skylake CPUs (2.4 GHz) with 192 GB of DDR4 DRAM, the HF model (664,724 grid cells) requires 4,032 CPU hours to complete, while the LF model (14,536 grid cells) requires only 48 CPU hours. Thus, by applying the downscaling approach to the LF ensemble simulations, our method provides an efficient way to evaluate the impact of the uncertainty in tropical cyclone (TC) predictions on the simulation of urban flooding. Figure 10 shows that compared to the single-member PGW simulation described in the above evaluation, a three-member ensemble of PGW simulations predicts higher peak inundation depths in the lower reaches of the Buffalo Bayou watershed, where population density is also the highest. In some areas, the difference in peak flood depth during the PGW event can exceed 1 m (Fig. 10b). Using the ensemble simulations, we can also calculate the likelihood of the areas where the PGW flood event poses significant or high risks to human safety (h>0.95 m; Russo et al., 2013). From the ensemble simulations, humans will very likely face significant risks to the flood water in the two reservoirs, river channels, and the nearby areas in Houston during the PGW flood event (Fig. 10c). In line with Fig. (10b), some simulations predict larger extents of the areas where the flood event would pose significant risks to human safety.
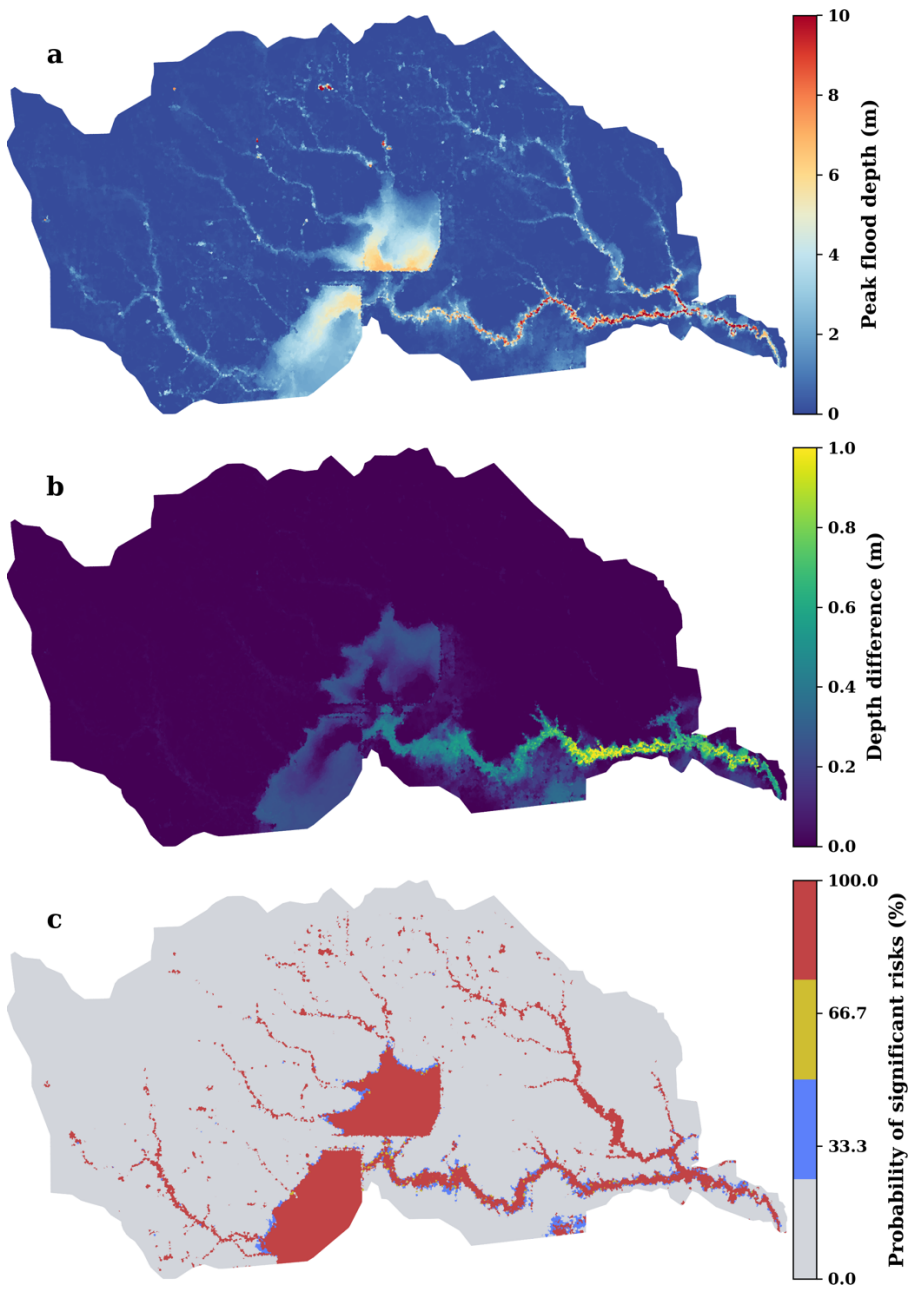
Figure 10. Projected peak flood depth of the PGW ensemble simulation (a), the difference of the projected peak flood depth between the PGW ensemble simulation and the selected PGW simulation (b), and the probability of significant risks to human safety by flood (c).

4 Discussions

4.1 Simulation of high-resolution river hydrodynamics

Our results demonstrate that the LSG model-based downscaling approach can provide efficient and accurate simulations of high-resolution river hydrodynamics at the computational cost of LF RHMs. To the best of our knowledge, this is one of the first studies to explore methods for fast and accurate simulations of high-resolution flow velocity in realistic cases, broadening the usefulness and relevance of recent rapid progress in hydrodynamic modeling, which still exclusively focuses on flooding (Carreau & Guinot, 2021; Xie et al., 2021; Zhou et al., 2021; Feng et al., 2023b; Fraehr et al., 2023b; Frame et al., 2024; Wing et al., 2024). With HF simulations of flow velocity, our understanding of not only instantaneous flood hazards but also longer time-scale environmental hazards, such as eutrophication and pollution, can be greatly advanced. More broadly, the new method can contribute to the development of fully coupled atmosphere-land-river-ocean ESMs, which will be discussed in detail in Section 4.2. It is worth noting that the study watersheds of Fraehr et al. (2023a, 2023b) differ from this study in land use and climate. The two Australian watersheds in Fraehr et al. (2023a, 2023b) are dominated by rural and natural landscapes and are less affected by TCs. The success of the LSG model in different domains underscores its broad geographical applicability.

The LSG model-based downscaling approach has two major advantages over neural network (NN)-based methods for high-resolution river hydrodynamic modeling. First, compared to NN-based methods (Tran et al., 2023), the training time of the LSG method is negligible, requiring only one expensive HF RHM simulation for training. Second, because physical laws have been explicitly coded in LF RHMs and implicitly complied with in the spatial interpolation process, the trained model can be expected to be transferable to future unseen climate conditions. These advantages make the approach well-suited for ensemble projections of future flooding, which are crucial for robust assessment of flood adaptation and mitigation (Fig. 10) given the substantial uncertainty of TC projections (Fig. 3). Another potential strength of our approach is that it can directly benefit from future advances in RHMs. The development of better RHMs will provide more accurate LF and HF simulations of river hydrodynamics for LSG model training, helping to reduce downscaling uncertainty (Fraehr et al., 2023a).

While a well-trained LSG model can be applied to unseen climate conditions, it is not free from re-training. For instance, without re-training, an LSG model is unlikely to handle changes in land use and geographical features, such as geomorphological changes in river channels and river flow modifications related to reservoirs. Additionally, our training strategy, which trains the LSG model only with data from the Harvey flood event, may not be effective in more complex cases where floods are not always driven by TCs. For instance, the main flood mechanisms in the U.S. Mid-Atlantic watersheds include both rain-on-snow (ROS) and snowmelt events that mainly occur in high-latitude areas (e.g., 1996 ROS Flood), and heavy rainfall from tropical cyclones (e.g., Hurricane Irene in 2011), extratropical systems, and convective systems (Smith et al., 2010; Li et al., 2021; Sun et al., 2024). For such cases, it is necessary to follow the training procedure of Fraehr et al. (2023a), selecting multiple representative flood events of different types for training. Since the number of flood mechanisms

is limited, we expect that the computational demand will still be manageable even if the LSG model is applied to a watershed with diverse flood generation processes.

395 Our study reveals that the downscaling accuracy of flow velocity is lower than that of flow depth. This is because the dynamics of flow velocity are more nonlinear, which induces significantly larger dimensionality-reduction errors in the downscaling process (Fig. 8). Accordingly, we introduced a regionalized training procedure to improve the downscaled flow velocity in focused areas (Fig. 9). This procedure does not significantly increase the computational cost of the LSG model because it does not require any new RHM runs. We envision that this strategy can be particularly useful for simulating river hydrodynamics in geographical areas that need more careful flood risk assessments, such as schools, hospitals, critical
400 infrastructures, energy facilities, and Superfund sites (Brand et al., 2018).

The LSG model error ER_{LSG} primarily depends on the performance of the Sparse GP model in mapping LF ECs to HF ECs. Besides the Sparse GP model, other data-driven models, such as Multilayer Perceptrons and Artificial Neural Networks, can also be used to establish the complex relationships between ECs (Carreau & Guinot, 2021). Future research on implementing other data-driven models to reduce ER_{LSG} is also worth exploring.

405 The LF model used in this study is about 84 times faster than the HF model, which is significantly more efficient than the LF model adopted by Fraehr et al. (2023a) that is only 12 times faster. Also, our LF model achieves a larger acceleration rate than the theoretical boost rate when considering the reduction in the number of grid cells ($\frac{664,724}{14,536} \approx 46$). The improved efficiency indicates that the OFM RHM has taken advantage of fewer computational units and longer time steps according to the Courant–Friedrichs–Lewy convergence criteria in the simulations. Furthermore, the results underscore the usefulness of
410 our approach for flood risk assessment, which needs hundreds or thousands of ensemble model runs for uncertainty quantification (Wu et al., 2020), for which the configuration of Fraehr et al. (2023a) cannot provide due to its inefficient LF simulations.

4.2 Coupling large-scale hydrodynamical processes with local processes in river models

It is challenging to represent other physical, chemical, and biological processes beyond river discharge in large-scale
415 river models. This is mainly because, by sacrificing process and resolution accuracy for computational efficiency, these models cannot provide accurate simulations of high-resolution flow depth and velocity necessary for calculating local dynamics important for fluvial processes (Bertagni et al., 2024), such as sediment settling velocity (Li et al., 2022), bottom shear stress and diffusivity (Chen et al., 2023), and greenhouse gas outgassing velocity (Ulseth et al., 2019). By accurately and efficiently simulating high-resolution flow depth and velocity, our downscaling approach provides an opportunity to bridge the gaps
420 between large-scale hydrodynamical processes and detailed local processes in river models. Specifically, we propose a two-way coupling scheme in large-scale river models (Fig. 11). In the first stage of each simulation cycle, a large-scale river model is used to simulate coarse-resolution flow depth and velocity and transport mass and momentum downstream. In the second stage, the LSG model-based approach is employed to downscale the simulated flow depth and velocity to fine resolutions. In

the third stage, high-resolution hydrodynamics are used to drive detailed physical, chemical, and biological models, such as the PFLOTRAN model for geochemistry (Hammond et al., 2012) and the GAIA model for sediment (Tassi et al., 2023), to simulate the sources and sinks of the represented tracers. In the final stage, the sources and sinks calculated in the fine-resolution mesh are upscaled to the coarse-resolution mesh of the large-scale river model and used to update the concentrations of the represented tracers.

An outstanding weakness of existing ESMs is that they ignore the lateral biogeochemical fluxes in the land-river-ocean continuum and therefore do not close the global biogeochemical cycles (Regnier et al., 2022). By implementing this new paradigm of river modeling in ESMs, land, river, and ocean biogeochemistry will be fully coupled, helping to close the global biogeochemical cycles. To achieve this vision, future research must focus on extending the LSG model-based approach to downscale 1-D river models to 2-D fine-resolution meshes. This is because, despite the prospect of 2-D large-scale river models running on GPU-based supercomputers, 1-D river models will likely still be the default configuration in ESMs in the near future (Telteu et al., 2021). We envision that the potential challenges could include the alignment of 1-D and 2-D unstructured meshes and the interpolation of simulated 1-D river hydrodynamics onto 2-D meshes.
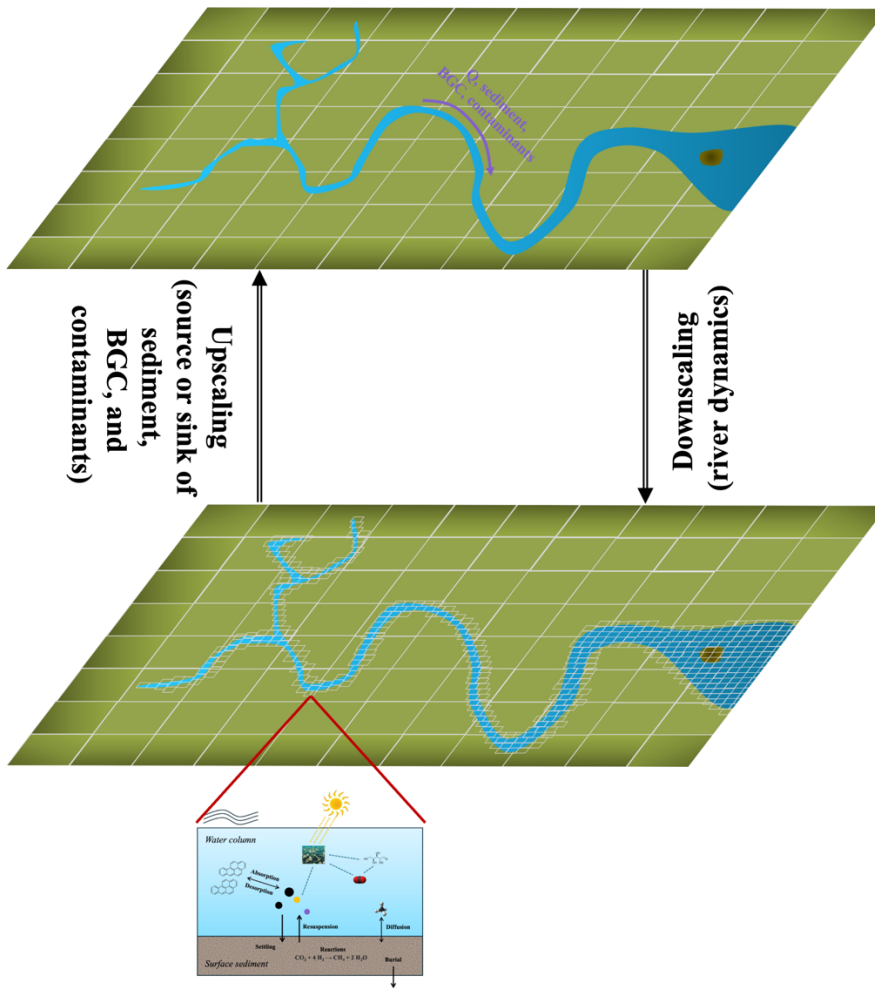
Figure 11. A schematic illustration of coupling large-scale hydrodynamical processes that are simulated in coarse resolution with local physical, chemical, and biological processes that are simulated in fine resolution in river models.

5 Conclusion

In this study, we developed a downscaling approach based on the LSG model to achieve fast and accurate simulations of high-resolution river flow depth and velocity. Our test of TC-induced flood events in an urban watershed in Houston demonstrates the effectiveness and efficiency of the downscaling method, as the simulation errors in the LF RHM are greatly reduced, without additional computational costs. We further indicated that the simulation error of the downscaled flow velocity can be reduced by employing regionalized training of the LSG model for selected focused areas. As one of the first studies to explore high-fidelity and efficient flow velocity simulations in realistic cases, our research can help broaden the usefulness and relevance of the recent rapid progress in hydrodynamic modeling, which still exclusively focuses on flooding. More importantly, the downscaling approach provides an opportunity to bridge the gaps between large-scale hydrodynamical

processes and local physical, chemical, and biological processes in river models, which could eventually help close the global

450 biogeochemical cycles in ESMs.

Code and data availability. The code and input data for this work can be publicly available at https://doi.org/10.5281/zenodo.14258083.

455 *Author contribution*. ZT, DX, and LRL designed the study. ZT developed the methodological framework and performed the formal analyses, validation, and visualization of the results. DX, ST, JM, and GB provided research resources. LRL performed funding acquisition and project administration. ZT wrote the original manuscript draft, and all co-authors reviewed and edited the manuscript.

460 *Competing interests*. The contact author has declared that none of the authors has any competing interests.

Acknowledgements. We thank the three anonymous reviewers for their constructive comments. This study was supported by the U.S. Department of Energy Advanced Scientific Computing Research (ASCR) program through the Multiphysics Simulations and Knowledge discovery through AI/ML technologies (MuSiKAL) project. It was also partly supported by the
465 Scientific Discovery through Advanced Computing 5 (Capturing the Dynamics of Compound Flooding in E3SM) and the Integrated Coastal Modeling (ICoM) project, funded by the U.S. Department of Energy, Office of Science, Office of Biological and Environmental Research as part of the Earth System Model Development (ESMD) and Regional and Global Model Analysis (RGMA) program areas, respectively. The Pacific Northwest National Laboratory (PNNL) is operated by Battelle for the U.S. Department of Energy under Contract DE-AC05-76RLO1830. All model simulations were performed using
470 resources available through (a) Research Computing at PNNL and (b) the National Energy Research Scientific Computing Center (NERSC), a U.S. Department of Energy Office of Science User Facility located at Lawrence Berkeley National Laboratory, operated under Contract No. DE-AC02-05CH11231 using NERSC award BER- ERCAP0027117.

References

Allen, G. H. and Pavelsky, T. M.: Global extent of rivers and streams, Science, 361, 585–588, 2018.

475 Balaguru, K., Foltz, G. R., and Leung, L. R.: Increasing magnitude of hurricane rapid intensification in the central and eastern tropical Atlantic, Geophys. Res. Lett., 45, 4238–4247, 2018.

Balay, S., Abhyankar, S., Adams, M., Brown, J., Brune, P., Buschelman, K., et al.: PETSc User's Manual, 2019.

Bates, P. D.: Flood inundation prediction, Annu. Rev. Fluid Mech., 54, 287–315, 2022.

Battin, T. J., Lauerwald, R., Bernhardt, E. S., Bertuzzo, E., Gener, L. G., Hall, R. O., Hotchkiss, E. R., Maavara, T., Pavelsky,
480 T. M., Ran, L., Raymond, P., Rosentreter, J. A., and Regnier, P.: River ecosystem metabolism and carbon biogeochemistry in a changing world, Nature, 613, 449–459, 2023.

Begnudelli, L. and Sanders, B. F.: Unstructured grid finite-volume algorithm for shallow-water flow and scalar transport with wetting and drying, J. Hydraul. Eng., 132, 371–384, 2006.

Bermúdez, M., Cea, L., Van Uytven, E., Willems, P., Farfán, J., and Puertas, J.: A robust method to update local river inundation maps using global climate model output and weather typing based statistical downscaling, Water Resour. Manag., 34, 4345–4362, 2020.

Bertagni, M. B., Regnier, P., Yan, Y., and Porporato, A.: A dimensionless framework for the partitioning of fluvial inorganic carbon, Geophys. Res. Lett., 51, e2024GL111310, 2024.

Brand, J. H., Spencer, K. L., O'Shea, F. T., and Lindsay, J. E.: Potential pollution risks of historic landfills on low-lying coasts and estuaries, WIREs Water, 5, e1264, 2018.

Caldwell, P. M., Terai, C. R., Hillman, B., Keen, N. D., Bogenschutz, P., Lin, W., Beydoun, H., Taylor, M., Bertagna, L., Bradley, A. M., Clevenger, T. C., Donahue, A. S., Eldred, C., Foucar, J., Golaz, J.-C., Guba, O., Jacob, R., Johnson, J., Krishna, J., Liu, W., Pressel, K., Salinger, A. G., Singh, B., Steyer, A., Ullrich, P., Wu, D., Yuan, X., Shpund, J., Ma, H.-Y., and Zender, C. S.: Convection-permitting simulations with the E3SM global atmosphere model, J. Adv. Model. Earth Syst., 13, e2021MS002544, 2021.

Carreau, J. and Guinot, V.: A PCA spatial pattern based artificial neural network downscaling model for urban flood hazard assessment, Adv. Water Resour., 147, 103821, 2021.

Chen, K., Chen, H., Zhou, C., Huang, Y., Qi, X., Shen, R., et al.: Comparative analysis of surface water quality prediction performance and identification of key water parameters using different machine learning models based on big data, Water Res., 171, 115454, 2020.

Chen, K., Yang, S., Roden, E. E., Chen, X., Chang, K.-Y., Guo, Z., et al.: Influence of vertical hydrologic exchange flow, channel flow, and biogeochemical kinetics on CH_4 emissions from rivers, Water Resour. Res., 59, e2023WR035341, 2023.

Denis, B., Laprise, R., Caya, D., and Côté, J.: Downscaling ability of one-way nested regional climate models: the Big-Brother Experiment, Climate Dynamics, 18, 627–646, 2002.

Donahue, A. S., Caldwell, P. M., Bertagna, L., Beydoun, H., Bogenschutz, P. A., Bradley, A. M., Clevenger, T. C., Foucar, J., Golaz, C., Guba, O., Hannah, W., Hillman, B. R., Johnson, J. N., Keen, N., Lin, W., Singh, B., Sreepathi, S., Taylor, M. A., Tian, J., Terai, C. R., Ullrich, P. A., Yuan, X., and Zhang, Y.: To exascale and beyond—The Simple Cloud-Resolving E3SM Atmosphere Model (SCREAM), a performance portable global atmosphere model for cloud-resolving scales, J. Adv. Model. Earth Syst., 16, e2024MS004314, 2024.

Emanuel, K.: Assessing the present and future probability of Hurricane Harvey's rainfall, Proc. Natl. Acad. Sci., 114, 12681–12684, 2017.

Engwirda, D.: JIGSAW-GEO (1.0): locally orthogonal staggered unstructured grid generation for general circulation modelling on the sphere, Geosci. Model Dev., 10, 2117–2140, 2017.

Feng, D., Tan, Z., Engwirda, D., Liao, C., Xu, D., Bisht, G., Zhou, T., Li, H.-Y., and Leung, L. R.: Investigating coastal backwater effects and flooding in the coastal zone using a global river transport model on an unstructured mesh, Hydrol. Earth Syst. Sci., 26, 5473–5491, 2022.

Feng, D., Tan, Z., Xu, D., and Leung, L. R.: Understanding the compound flood risk along the coast of the contiguous United States, Hydrol. Earth Syst. Sci., 27, 3911–3934, 2023a.

Feng, D., Tan, Z., and He, Q: Physics-informed neural networks of the Saint-Venant equations for downscaling a large-scale river model, Water Resour. Res., 59, e2022WR033168, 2023b.

Feng, D., Tan, Z., Engwirda, D., Wolfe, J. D., Xu, D., Liao, C., Bisht, G., Benedict, J. J., Zhou, T., Li, H., and Leung, L. R.: Simulation of compound flooding using river-ocean two-way coupled E3SM ensemble on variable-resolution meshes, J. Adv. Model. Earth Syst., 2024.

Fraehr, N., Wang, Q. J., Wu, W., and Nathan, R.: Upskilling low-fidelity hydrodynamic models of flood inundation through
525   Spatial analysis and Gaussian Process learning, Water Resour. Res., 58, e2022WR032248, 2022.

Fraehr, N., Wang, Q. J., Wu, W., and Nathan, R.: Development of a fast and accurate hybrid model for floodplain inundation
simulations, Water Resour. Res., 59, e2022WR033836, 2023a.

Fraehr, N., Wang, Q. J., Wu, W., and Nathan, R.: Supercharging hydrodynamic inundation models for instant flood
insight, Nat. Water, 1, 835–843, 2023b.

530   Frame, J. M., Nair, T., Sunkara, V., Popien, P., Chakrabarti, S., Anderson, T., et al.: Rapid inundation mapping using the US
National Water Model, satellite observations, and a convolutional neural network, Geophys. Res. Lett., 51, e2024GL109424,
2024.

Freer, J., Beven, K. J., Neal, J., Schumann, G., Hall, J., and Bates, P.: Flood risk and uncertainty, in: Risk and Uncertainty
Assessment for Natural Hazards, Cambridge, Cambridge University Press, pp. 190–233, 2011.

535   Gadgil, A.: Drinking water in developing countries, Annu. Rev. Energy Environ., 23, 253–286, 1998.

Gao, S., Huang, Y., Zhang, S., Han, J., Wang, G., Zhang, M., and Lin, Q.: Short-term runoff prediction with GRU and LSTM
networks without requiring time step optimization during sample generation, J. Hydrol., 589, 125188, 2020.

Gupta, H. V., Kling, H., Yilmaz, K. K., and Martinez, G. F.: Decomposition of the mean squared error and NSE performance
criteria: Implications for improving hydrological modelling, J. Hydrol., 377, 80–91, 2009.

540   Ha, S., Liu, D., and Mu, L.: Prediction of Yangtze River streamflow based on deep learning neural network with El Niño–
Southern Oscillation, Sci. Rep., 11, 11738, 2021.

Haddeland, I., Lettenmaier, D. P., and Skaugen, T.: Effects of irrigation on the water and energy balances of the Colorado and
Mekong river basins, J. Hydrol., 324, 210–223, 2006.

Hammond, G. E., Lichtner, P. C., Lu, C., and Mills, R. T.: PFLOTRAN: Reactive flow and transport code for use on laptops
545   to leadership-class supercomputers, Groundwater Reactive Transport Models, 5, 141–159, 2012.

He, Q., Barajas-Solano, D., Tartakovsky, G., and Tartakovsky, A. M.: Physics-informed neural networks for multiphysics data
assimilation with application to subsurface transport, Adv. Water Res., 141, 103610, 2020.

Hersbach, H., Bell, B., Berrisford, P., Hirahara, S., Horányi, A., Muñoz-Sabater, J., et al.: The ERA5 global reanalysis, Q. J.
Roy. Meteor. Soc., 146, 1999–2049, 2020.

550   Hostache, R., Hissler, C., Matgen, P., Guignard, C., and Bates, P.: Modelling suspended-sediment propagation and related
heavy metal contamination in floodplains: a parameter sensitivity analysis, Hydrol. Earth Syst. Sci., 18, 3539–3551, 2014.

Hu, X., Shi, L., Lin, G., and Lin, L.: Comparison of physical-based, data-driven and hybrid modeling approaches for
evapotranspiration estimation, J. Hydrol., 601, 126592, 2021.

Huang, S., Xia, J., Wang, Y., Wang, W., Zeng, S., She, D., and Wang, G.: Coupling machine learning into hydrodynamic
555   models to improve river modeling with complex boundary conditions, Water Resour. Res., 58, e2022WR032183, 2022.

Ibáñez, C. and Peñuelas, J.: Changing nutrients, changing rivers, Science, 365, 637–638, 2019.

IPCC.: Climate change 2021: The physical science basis. Contribution of working group I to the sixth assessment report of the
intergovernmental panel on climate change, C. U. Press., 2021.

Ivanov, V. Y., Xu, D., Dwelle, M. C., Sargsyan, K., Wright, D. B., Katopodes, N., Kim, J., Tran, V. N., Warnock, A., Fatichi,
560   S., Burlando, P., Caporali, E., Restrepo, P., Sanders, B. F., Chaney, M. M., Nunes, A. M. B., Nardi, F., Vivoni, E. R.,
Istanbulluoglu, E., Bisht, G., and Bras, R. L.: Breaking down the computational barriers to real-time urban flood forecasting,
Geophys. Res. Lett., 48, e2021GL093585, 2021.

Kaiser, H. F.: The application of electronic computers to factor analysis, Educ. Psychol. Meas., 20, 141–151, 1960.

Karniadakis, G. E., Kevrekidis, I. G., Lu, L., Perdikaris, P., Wang, S., and Yang, L.: Physics-informed machine learning, Nat. Rev. Phys., 3, 422–440, 2021.

Kim, D.-W., Chung, E. G., Kim, K., and Kim, Y.: Impact of riverbed topography on hydrology in small watersheds using soil and water assessment tool, Environ. Model. Softw., 152, 105383, 2022.

Kim, J., Warnock, A., Ivanov, V. Y., and Katopodes, N. D.: Coupled modeling of hydrologic and hydrodynamic processes including overland and channel flow, Adv. Water Resour., 37, 104–126, 2012.

Knoben, W. J. M., Freer, J. E., and Woods, R. A.: Technical note: Inherent benchmark or not? Comparing Nash–Sutcliffe and Kling–Gupta efficiency scores, Hydrol. Earth Syst. Sci., 23, 4323–4331, 2019.

Konapala, G., Kao, S.-C., Painter, S. L., and Lu, D.: Machine learning assisted hybrid models can improve streamflow simulation in diverse catchments across the conterminous US, Environ. Res. Lett., 15, 104022, 2020.

Li, H., Wigmosta, M. S., Wu, H., Huang, M., Ke, Y., Coleman, A. M., and Leung, L. R.: A physically based runoff routing model for land surface and earth system models, J. Hydrometeorol., 14, 808–828, 2013.

Li, H.-Y., Tan, Z., Ma, H., Zhu, Z., Abeshu, G. W., Zhu, S., Cohen, S., Zhou, T., Xu, D., and Leung, L. R.: A new large-scale suspended sediment model and its application over the United States, Hydrol. Earth Syst. Sci., 26, 665–688, 2022.

Li, J., Qian, Y., Leung, L. R., and Feng, Z.: Summer mean and extreme precipitation over the Mid-Atlantic region: Climatological characteristics and contributions from different precipitation types, J. Geophys. Res.-Atmos., 126, e2021JD035045, 2021.

Liang, C., Li, H., Lei, M., and Du, Q.: Dongting lake water level forecast and its relationship with the three gorges dam based on a long short-term memory network, Water, 10, 1389, 2018.

Liao, C., Zhou, T., Xu, D., Barnes, R., Bisht, G., Li, H.-Y., Tan, Z., Tesfa, T., Duan, Z., Engwirda, D., and Leung, L. R.: Advances in hexagon mesh-based flow direction modeling, Adv. Water Resour., 160, 104099, 2022.

Luo, X., Li, H. Y., Leung, L. R., Tesfa, T. K., Getirana, A., Papa, F., and Hess, L. L.: Modeling surface water dynamics in the Amazon Basin using MOSART-Inundation v1. 0: impacts of geomorphological parameters and river flow representation, Geosci. Model Dev., 10, 1233–1259, 2017.

Macklin, M. G., Thomas, C. J., Mudbhatkal, A., Brewer, P. A., Hudson-Edwards, K. A., Lewin, J., Scussolini, P., Eilander, D., Lechner, A., Owen, J., Bird, G., Kemp, D., and Mangalaa, K. R.: Impacts of metal mining on river systems: a global assessment, Science, 381, 1345–1350, 2023.

Mahesh, R. B., Leandro, J., and Lin, Q.: Physics informed neural network for spatial-temporal flood forecasting, in: Climate Change and Water Security, Springer, pp. 77–91, 2022.

Mao, Y., Zhou, T., Leung, L. R., Tesfa, T. K., Li, H.-Y., Wang, K., Tan, Z., and Getirana, A.: Flood inundation generation mechanisms and their changes in 1953–2004 in global major river basins, J. Geophys. Res.-Atmos., 124, 11672–11692, 2019.

Mishra, V. and Shah, H.: Hydroclimatological perspective of the Kerala Flood of 2018, J. Geol. Soc. India, 92, 645–650, 2018.

North, G. R., Bell, T. L., Cahalan, R. F., and Moeng, F. J.: Sampling errors in the estimation of empirical orthogonal functions, Mon. Weather Rev., 110, 699–706, 1982.

Oki, T. and Kanae, S.: Global hydrological cycles and world water resources, Science, 313, 1068–1073, 2006.

Rasmussen, C. E. and Williams, C. K. I.: Gaussian processes for machine learning, MIT Press, 2006.

Raymond, P. A., Saiers, J. E., and Sobczak, W. V.: Hydrological and biogeochemical controls on watershed dissolved organic matter transport: Pulse-shunt concept, Ecology, 97, 5–16, 2016.

Razavi, S., Tolson, B. A., and Burn, D. H.: Review of surrogate modeling in water resources, Water Resour. Res., 48, W07401, 2012.

Regnier, P., Resplandy, L., Najjar, R. G., and Ciais, P.: The land-to-ocean loops of the global carbon cycle, Nature, 603, 401–410, 2022.

Rocher-Ros, G., Stanley, E. H., Loken, L. C., Casson, N. J., Raymond, P. A., Liu, S., Amatulli, G., and Sponseller, R. A.: Global methane emissions from rivers and streams, Nature, 621, 530–535, 2023.

Russo, B., Gómez, M., and Macchione, F.: Pedestrian hazard criteria for flooded urban areas, Nat. Hazards, 69, 251–265, 2013.

Saha, G. K., Rahmani, F., Shen, C., Li, L., and Cibin, R.: A deep learning-based novel approach to generate continuous daily stream nitrate concentration for nitrate data-sparse watersheds, Sci. Total Environ., 878, 162930, 2023.

Schmutz, S. and Moog, O.: Riverine ecosystem management: Science for governing towards a sustainable future, in Schmutz, S. and Sendzimir, J. (eds), Springer International Publishing, Cham, pp. 111–127, 2018.

Schrapffer, A., Sörensson, A., Polcher, J., and Fita, L.: Benefits of representing floodplains in a Land Surface Model: Pantanal simulated with ORCHIDEE CMIP6 version, Clim. Dyn., 55, 1303–1323, 2020.

Shabani, A., Woznicki, S. A., Mehaffey, M., Butcher, J., Wool, T. A., and Whung, P. Y.: A coupled hydrodynamic (HEC-RAS 2D) and water quality model (WASP) for simulating flood-induced soil, sediment, and contaminant transport, J. Flood Risk Manag., 14, e12747, 2021.

Sherwood, S. C., Bony, S., and Dufresne, J.-L.: Spread in model climate sensitivity traced to atmospheric convective mixing, Nature, 505, 37–42, 2014.

Sikorska-Senoner, A. E. and Quilty, J. M.: A novel ensemble-based conceptual-data-driven approach for improved streamflow simulations, Environ. Model. Softw., 143, 105094, 2021.

Smith, J. A., Baeck, M. L., Villarini, G., and Krajewski, W. F.: The hydrology and hydrometeorology of flooding in the Delaware River Basin, J. Hydrometeorol., 11, 841–859, 2010.

Sukhodolov, A. N., Shumilova, O. O., Constantinescu, G. S., Lewis, Q. W., and Rhoads, B. L.: Mixing dynamics at river confluences governed by intermodal behaviour, Nat. Geosci., 16, 89–93, 2023.

Sun, N., Wigmosta, M. S., Yan, H., Eldardiry, H., Yang, Z., Deb, M., Wang, T., and Judi, D.: Amplified Extreme Floods and Shifting Flood Mechanisms in the Delaware River Basin in Future Climates, Earth's Future, 12, e2023EF003868, 2024.

Syvitski, J. P. M., Vörösmarty, C. J., Kettner, A. J., and Green, P.: Impact of humans on the flux of terrestrial sediment to the global coastal ocean, Science, 308, 376–380, 2005.

Tassi, P., Benson, T., Delinares, M., Fontaine, J., Huybrechts, N., Kopmann, R., Pavan, S., Pham, C. T., Taccone, F., and Walther, R.: GAIA - a unified framework for sediment transport and bed evolution in rivers, coastal seas and transitional waters in the TELEMAC-MASCARET modelling system, Environ. Model. Softw., 159, 105544, 2023.

Telteu, C.-E., Müller Schmied, H., Thiery, W., Leng, G., Burek, P., Liu, X., Boulange, J. E. S., Andersen, L. S., Grillakis, M., Gosling, S. N., Satoh, Y., Rakovec, O., Stacke, T., Chang, J., Wanders, N., Shah, H. L., Trautmann, T., Mao, G., Hanasaki, N., Koutroulis, A., Pokhrel, Y., Samaniego, L., Wada, Y., Mishra, V., Liu, J., Döll, P., Zhao, F., Gädeke, A., Rabin, S. S., and Herz, F.: Understanding each other's models: an introduction and a standard representation of 16 global water models to support intercomparison, improvement, and communication, Geosci. Model Dev., 14, 3843–3878, 2021.

Teng, J., Jakeman, A. J., Vaze, J., Croke, B. F. W., Dutta, D., and Kim, S.: Flood inundation modelling: A review of methods, recent advances and uncertainty analysis, Environ. Model. Softw., 90, 201–216, 2017.

Tran, V. N., Ivanov, V. Y., Xu, D., and Kim, J.: Closing in on hydrologic predictive accuracy: Combining the strengths of high-fidelity and physics-agnostic models, Geophys. Res. Lett., 50, e2023GL104464, 2023.

Ulseth, A. J., Hall Jr, R. O., Boix Canadell, M., Madinger, H. L., Niayifar, A., and Battin, T. J.: Distinct air–water gas exchange regimes in low- and high-energy streams, Nat. Geosci., 12, 259–263, 2019.

645 Van Oldenborgh, G. J., Van Der Wiel, K., Sebastian, A., Singh, R., Arrighi, J., Otto, F., Haustein, K., Li, S., Vecchi, G., and Cullen, H.: Attribution of extreme rainfall from Hurricane Harvey, August 2017, Environ. Res. Lett., 12, 124009, 2017.

Wang, S.-Y. S., Zhao, L., Yoon, J.-H., Klotzbach, P., and Gillies, R. R.: Quantitative attribution of climate effects on Hurricane Harvey's extreme rainfall in Texas, Environ. Res. Lett., 13, 054014, 2018.

Wilby, R. L. and Dawson, C. W.: The statistical downscaling model: Insights from one decade of application, Int. J. Climatol.,
650 33, 1707–1719, 2013.

Wing, O. E. J., Bates, P. D., Quinn, N. D., Savage, J. T. S., Uhe, P. F., Cooper, A., Collings, T. P., Addor, N., Lord, N. S., Hatchard, S., Hoch, J. M., Bates, J., Probyn, I., Himsworth, S., Rodríguez González, J., Brine, M. P., Wilkinson, H., Sampson, C. C., Smith, A. M., Neal, J. C., and Haigh, I. D.: A 30 m global flood inundation model for any climate scenario, Water Resour. Res., 60, e2023WR036460, 2024.

655 Wu, H., Kimball, J. S., Mantua, N., and Stanford, J.: Automated upscaling of river networks for macroscale hydrological modeling, Water Resour. Res., 47, W03517, 2011.

Wu, W. Y., Emerton, R., Duan, Q. Y., Wood, A. W., Wetterhall, F., and Robertson, D. E.: Ensemble flood forecasting: Current status and future opportunities, WIREs Water, 7, e1432, 2020.

Wunsch, A., Liesch, T., and Broda, S.: Deep learning shows declining groundwater levels in Germany until 2100 due to climate
660 change, Nat. Commun., 13, 1221, 2022.

Xie, S., Wu, W., Mooser, S., Wang, Q. J., Nathan, R., and Huang, Y.: Artificial neural network based hybrid modeling approach for flood inundation modeling, J. Hydrol., 592, 125605, 2021.

Xu, D., Bisht, G., Zhou, T., Leung, L. R., and Pan, M.: Development of land-river two-way hydrologic coupling for floodplain inundation in the Energy Exascale Earth System Model, J. Adv. Model. Earth Syst., 14, e2021MS002772, 2022.

665 Xu, D., Bisht, G., Engwirda, D., Feng, D., Tan, Z., and Ivanov, V. Y.: Uncertainties in simulating flooding during Hurricane Harvey using 2D shallow water equations, Water Resour. Res., 61, e2024WR038032, 2025.

Yamazaki, D., Kanae, S., Kim, H., and Oki, T.: A physically based description of floodplain inundation dynamics in a global river routing model, Water Resour. Res., 47, 2010WR009726, 2011.

Yang, L., Smith, J., Liu, M., and Baeck, M. L.: Extreme rainfall from Hurricane Harvey (2017): Empirical intercomparisons
670 of WRF simulations and polarimetric radar fields, Atmos. Res., 223, 114–131, 2019.

Yang, S., Yang, D., Chen, J., and Zhao, B.: Real-time reservoir operation using recurrent neural networks and inflow forecast from a distributed hydrological model, J. Hydrol., 579, 124229, 2019.

Young, C.-C., Liu, W.-C., and Wu, M.-C.: A physically based and machine learning hybrid approach for accurate rainfall-runoff modeling during extreme typhoon events, Appl. Soft Comput., 53, 205–216, 2017.

675 Zhang, D., Lin, J., Peng, Q., Wang, D., Yang, T., Sorooshian, S., et al.: Modeling and simulating of reservoir operation using the artificial neural network, support vector regression, deep learning algorithm, J. Hydrol., 565, 720–736, 2018.

Zhang, J., Howard, K., Langston, C., Kaney, B., Qi, Y., Tang, L., et al.: Multi-Radar Multi-Sensor (MRMS) Quantitative Precipitation Estimation: Initial Operating Capabilities, Bull. Am. Meteorol. Soc., 97, 621–638, 2016.

Zhang, Q., Ye, X., Werner, A. D., Li, Y., Yao, J., Li, X., and Xu, C.: An investigation of enhanced recessions in Poyang Lake:
680 Comparison of Yangtze River and local catchment impacts, J. Hydrol., 517, 425–434, 2014.

Zhou, Y., Wu, W., Nathan, R., and Wang, Q. J.: A rapid flood inundation modelling framework using deep learning with spatial reduction and reconstruction, Environ. Model. Softw., 143, 105112, 2021.